

ON THE ORIGIN OF ENERGY BARRIERS IN THE EXCITED STATES OF He<sub>2</sub><sup>†</sup>

S.L. GUBERMAN and W.A. GODDARD III

*Arthur Amos Noyes Laboratory of Chemical Physics<sup>‡</sup>, California Institute of Technology,  
Pasadena, California 91109, USA*

Received 10 March 1972

The A <sup>1</sup>Σ<sub>u</sub><sup>+</sup> and C <sup>1</sup>Σ<sub>g</sub><sup>+</sup> states of He<sub>2</sub> have been examined using self-consistent (spatially projected) generalized valence bond (GVB) wavefunctions. We find both states to have humps (0.06 and 0.22 eV, respectively) at large *R* (3.1 Å and 2.1 Å, respectively). The repulsive nature of these states at large *R* results from non-bonding interactions between the singlet pairs of orbitals located on different centers. For *R* smaller than the size of the excited He orbital (2s or 2p), the state becomes attractive if the symmetry is such that the wavefunction can build in attractive He<sub>2</sub><sup>‡</sup>(<sup>2</sup>Σ<sub>u</sub><sup>+</sup>) character.

## 1. Introduction

Although the potential curve for the ground state of He<sub>2</sub> is primarily repulsive (exhibiting a van der Waals minimum of 0.000875 eV at 2.9 Å) [1], many excited states are known to be bound with respect to the corresponding excited states of the separated atoms. A particularly interesting feature of this system is that many of the potential curves are repulsive at large internuclear distance, *R*, leading to a hump (maximum) at intermediate *R* (1.5 to 3.5 Å). For smaller *R* the energy decreases rapidly, leading to a minimum around 1 Å with a binding energy of up to 2 eV. Here our primary objective is to examine the origin of these humps in the potential curves.

## 2. The wavefunctions

The Hartree–Fock (HF) method for electronic wavefunctions leads to orbitals in terms of which the wavefunction may be readily interpreted, but it also leads to an improper description of many excited states at large *R*. The configuration interaction (CI)

method can lead to a proper description of the potential curves but cannot be interpreted as easily as HF. Here we use wavefunctions closely akin to valence bond (VB) wavefunctions except that a different orbital is used for each electron, we solve for all orbitals self-consistently at each internuclear distance, and there are no orthogonality constraints between orbitals. Such wavefunctions are referred to here as generalized valence bond (GVB) wavefunctions, or more specifically, as spatially projected G1 wavefunctions<sup>†</sup>.

In this description the wavefunction for an excited singlet state of the He atom is described as

$$\alpha \{ [\phi_{\bar{c}}(1)\phi_v(2) + \phi_v(1)\phi_{\bar{c}}(2)] \alpha\beta \}, \quad (1)$$

where  $\alpha$  is the antisymmetrizer and denoted as in fig. 1a. Here  $\bar{c}$  is a 1s-like core orbital and *v* is the excited orbital (*v* = 2s for the 2 <sup>1</sup>S state and *v* = 2p for the 2 <sup>1</sup>P state). Orbital  $\phi_{\bar{c}}$  is very nearly the same for the various states of the He atom. The ground state also has the form in (1) but in this case both orbitals are 1s-like core orbitals.

At large *R* the GVB wavefunction for the ground

<sup>†</sup> For a discussion of the G1 method see ref. [2]. Here we use both the group operator  $G_1^{\gamma}$ , and a spatial projection operator and optimize the orbitals *after* projection. No orthogonality restrictions are made.

<sup>‡</sup> Partially supported by NSF grant GP-15423.

\* Contribution No. 4404.

$$\begin{array}{lll}
 \text{a. } \begin{array}{|c|} \hline \bar{c} \quad v \\ \hline \end{array} & \text{b. } \begin{array}{|c|c|} \hline c_l \quad c'_l \\ \hline c_r \quad c'_r \\ \hline \end{array} & \text{c. } \begin{array}{|c|c|} \hline c_l \quad c'_l \\ \hline \bar{c}_r \quad v_r \\ \hline \end{array} \\
 \\
 \text{d. } \begin{array}{|c|c|} \hline c_l \quad c'_l \\ \hline \bar{c}_r \quad v_r \\ \hline \end{array} & = & \begin{array}{|c|c|} \hline c_l \quad c'_l \\ \hline \bar{c}_r \quad v_r \\ \hline \end{array} + \begin{array}{|c|c|} \hline c_r \quad c'_r \\ \hline \bar{c}_l \quad v_l \\ \hline \end{array} \\
 \text{e. } \begin{array}{|c|c|} \hline c_l \quad c'_l \\ \hline \bar{c}_r \quad v_r \\ \hline \end{array} & = & \begin{array}{|c|c|} \hline c_l \quad c'_l \\ \hline \bar{c}_r \quad v_r \\ \hline \end{array} - \begin{array}{|c|c|} \hline c_r \quad c'_r \\ \hline \bar{c}_l \quad v_l \\ \hline \end{array} \\
 \text{f. } \begin{array}{|c|c|} \hline c_l \quad c'_l \\ \hline \bar{c}_r \quad v_r \\ \hline \end{array} & \approx & \begin{array}{|c|c|} \hline c_l \quad c'_l \\ \hline \bar{c}_r \quad v \\ \hline \end{array} + \begin{array}{|c|c|} \hline c_r \quad c'_r \\ \hline \bar{c}_l \quad v \\ \hline \end{array} \\
 \text{g. } \begin{array}{|c|c|} \hline c_l \quad c'_l \\ \hline \bar{c}_r \\ \hline \end{array} & = & \begin{array}{|c|c|} \hline c_l \quad c'_l \\ \hline \bar{c}_r \\ \hline \end{array} + \begin{array}{|c|c|} \hline c_r \quad c'_r \\ \hline \bar{c}_l \\ \hline \end{array} \\
 \text{h. } \begin{array}{|c|c|} \hline c_l \quad c'_l \\ \hline \bar{c}_r \\ \hline \end{array} & = & \begin{array}{|c|c|} \hline c_l \quad c'_l \\ \hline \bar{c}_r \\ \hline \end{array} - \begin{array}{|c|c|} \hline c_r \quad c'_r \\ \hline \bar{c}_l \\ \hline \end{array} \\
 \text{j. } \begin{array}{|c|c|} \hline c_l \quad c'_l \\ \hline \bar{c}_r \quad 2p\sigma_f \\ \hline \end{array} & \approx & \begin{array}{|c|c|} \hline c_l \quad c'_l \\ \hline \bar{c}_r \quad 2p\sigma \\ \hline \end{array} - \begin{array}{|c|c|} \hline c_r \quad c'_r \\ \hline \bar{c}_l \quad 2p\sigma \\ \hline \end{array} \\
 \text{k. } \begin{array}{|c|c|} \hline c_l \quad c'_l \\ \hline \bar{c}_r \quad 2p\sigma_f \\ \hline \end{array} & \approx & \begin{array}{|c|c|} \hline c_l \quad c'_l \\ \hline \bar{c}_r \quad 2p\sigma \\ \hline \end{array} + \begin{array}{|c|c|} \hline c_r \quad c'_r \\ \hline \bar{c}_l \quad 2p\sigma \\ \hline \end{array} \\
 \text{l. } \begin{array}{|c|c|} \hline c_l \quad c'_l \\ \hline \bar{c}_r \\ \hline v_r \\ \hline \end{array} & & 
 \end{array}$$

Fig. 1. The orbital couplings for various states of  $\text{He}_2$  and  $\text{He}_2^+$ .

state of  $\text{He}_2$  has the form

$$a \{ [\phi_{c_l} \phi_{c'_l} + \phi_{c'_l} \phi_{c_l}] [\phi_{c_r} \phi_{c'_r} + \phi_{c'_r} \phi_{c_r}] \alpha \beta \alpha \beta \}, \quad (2)$$

which we will denote as in fig. 1b, where  $\phi_{c_l}$  and  $\phi_{c'_l}$  are He  $1^1\text{S}$  orbitals on the left and  $\phi_{c_r}$  and  $\phi_{c'_r}$  are He  $1^1\text{S}$  orbitals on the right. For the case of an unexcited atom on the left and an excited one on the right, the wavefunction is denoted as in fig. 1c, where the  $\bar{c}$  is not quite equivalent to  $c$  or  $c'$ . The wavefunction of fig. 1c must be combined (as in figs. 1d, e) with another having inversions of these orbitals to obtain excited states having g or u symmetry. Thus for each internuclear distance we take the wavefunctions of the excited states of  $\text{He}_2$  to have the form in fig. 1d or 1e, and we solve for the orbitals self-consistently<sup>‡</sup>. As a result the orbitals for a g state (fig. 1d) are not

<sup>‡</sup> The basis set consisted of 6 s-type, 2 p-type, and 1 d-type contracted gaussians on each He constructed from a primitive set of 13 s-type, 6 p-type, and 4 d-type gaussians [3].

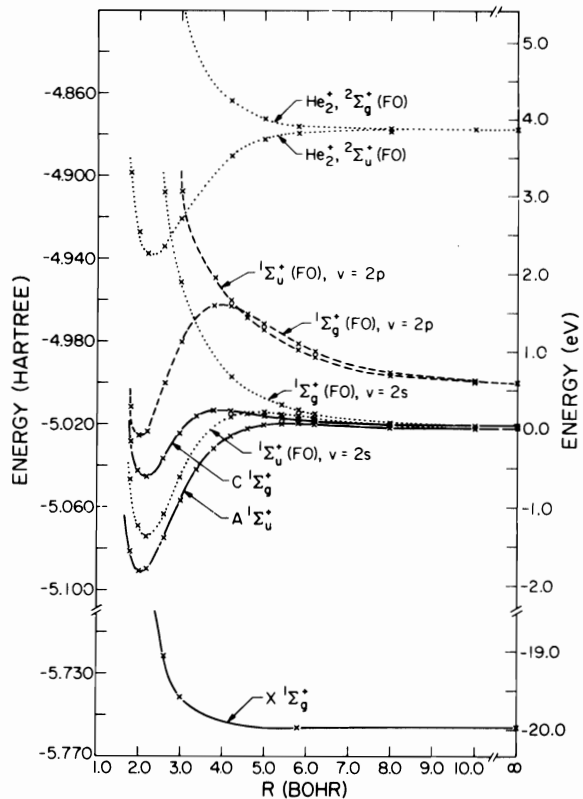


Fig. 2. The calculated energy curves. The solid lines indicate the fully self-consistent results for the  $X^1\Sigma_g^+$ ,  $A^1\Sigma_u^+$  and  $C^1\Sigma_g^+$  states of  $\text{He}_2$ . The dotted lines indicate the energies obtained using frozen orbitals (FO) for  $\text{He}_2^+$  and  $\text{He}_2$  with  $v = 2s$  for the latter. The dashed lines represent frozen orbital calculations for  $\text{He}_2$  with  $v = 2p$ .

exactly the same as those for the corresponding u state (fig. 1e). The core orbitals ( $c$ ,  $c'$ , and  $\bar{c}$ ) change only very slightly from state to state, and in our discussions we will ignore changes in the core orbitals.

### 3. Results

The calculated energy curves for the  $X^1\Sigma_g^+$  (fig. 1b),  $A^1\Sigma_u^+$  (fig. 1e), and  $C^1\Sigma_g^+$  (fig. 1d) states are shown in fig. 2<sup>†</sup>. (In the above wavefunctions  $c$ ,  $c'$ , and  $\bar{c}$ , and  $v$  differ slightly, of course, from state to

<sup>†</sup> For footnote see next page.

state.) For the  $A^1\Sigma_u^+$  state the GVB wavefunction accounts for about 72% or 80% of the binding energy (1.88 eV compared to 2.5 eV [4] or 2.34 eV [5], respectively) and leads to a value for the energy hump of 0.0607 eV, which is within the limits of several experimental determinations ( $0.05 \pm 0.01$  eV [5],  $0.03 \pm 0.03$  eV [6], 0.05 eV [4], 0.06 eV [7],  $0.049 \pm 0.01$  eV [8]). For the  $C^1\Sigma_g^+$  state the calculated hump is 0.2199 eV (there is not a good experimental estimate) and the calculated binding energy is 0.643 eV. The calculated  $R_e$  for the minima of the A and C states are 1.10 Å and 1.17 Å which are in fair agreement with the experimental values [9] 1.039 Å and 1.091 Å. We find the humps to occur at 3.09 Å for the A state and 2.09 Å for the C state. Experimental estimates are 3.1 Å [4, 8] and  $3.0 \pm 0.3$  Å [6] for the maximum in the A state. Such estimates are not available for the C state.

The GVB wavefunction typically accounts for only 80 to 90% of the  $D_e$  and usually leads to an  $R_e$  about 3–8% larger than the experimental value. However, these wavefunctions lead to an accurate description for intermediate  $R$ . We would expect our calculated humps to be of the order of 10 to 20% larger than the experimental values. There is not sufficient experience to estimate how close GVB predicts the location of potential humps, but we would expect it to be within 0.2 Å. Thus overall, the GVB results are in excellent agreement with values calculated from experimental results.

Allison et al. [10] used a 3 term CI wavefunction for the A state and obtained a hump of 0.084 eV at 3 Å. The GVB potential curve (while including no instantaneous correlation) is about 0.8 eV lower than that of Allison et al. Scott et al. [11] showed the possible unimportance of extensive instantaneous correlation in determining the hump height of the A state. Using both 4 and 17 term CI wavefunctions they ob-

† The orbitals for the ground state were allowed to split so that all the orbitals are different. However, for the points shown in fig. 2 this has only a negligible effect on the energy. Note also that the absence of an orthogonality constraint between the orbitals causes the C state to be 0.00076 au (0.02 eV) higher than the A state at  $R = \infty$ . This splitting does not occur for  $v = 2p$  since by symmetry the 2p orbital is orthogonal to the core orbitals on the same He at  $R = \infty$ .

‡ These are obtained from a parabolic fit of the appropriate calculated points. See fig. 2.

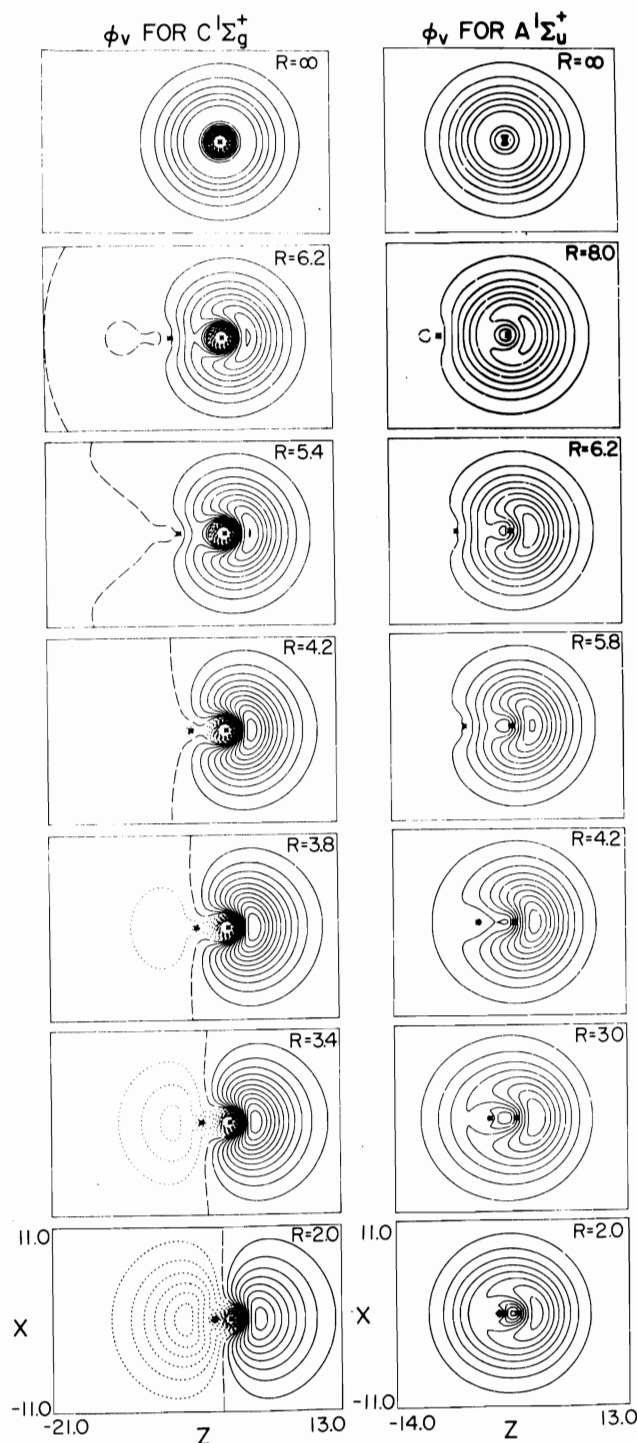


Fig. 3. The  $\phi_v$  orbital obtained from fully self-consistent GVB calculations on the  $A^1\Sigma_u^+$  and  $C^1\Sigma_g^+$  states of  $He_2$ . (All distances are in bohr.)

tained maxima of 0.154 and 0.153 eV, respectively. The only previous calculation on the C state showing an attractive minimum was by Browne [12]. He used a 3 term wavefunction and obtained a hump of about 0.7 eV at 2.4 Å. His potential curve was not smooth, showing a plateau between the maximum and the attractive minimum.

The core-like GVB orbitals do not change greatly with  $R$  and are not shown here. The valence orbitals change significantly with distance and are shown in fig. 3. Here we see that for both states  $\phi_v$  is essentially a He 2s orbital at large  $R$ . For the A state  $\phi_v$  changes only slightly with  $R$  and is still a 2s-like orbital at the minimum. However,  $\phi_v$  for the C state starts changing significantly near  $R = 4.2 a_0$  (2.2 Å) and by  $R_c$  is a 2p-like  $\sigma$  orbital. At  $R_c$  we can view these (and the higher) excited states of He<sub>2</sub> as Rydberg states with a He<sub>2</sub><sup>+</sup>-like core.

#### 4. Interpretation

A wavefunction of the form shown in fig. 1b consisting of a singlet pair on the left and a singlet pair on the right leads to a repulsive interaction in the energy curve (the well-known repulsion of closed shells) as long as van der Waals correlation effects are ignored. Thus considering the excited states in the form shown in fig. 1c, we would expect *all* of these states to be repulsive for large  $R$  (assuming the orbitals to be  $\sigma$ -like, i.e., not orthogonal by symmetry)<sup>†</sup>. This repulsive effect is determined by the magnitude of the two-center overlaps  $\langle l|r \rangle$ , and hence in the case that one orbital,  $\phi_{vR}$  or  $\phi_{vL}$ , is much more diffuse than the others, the terms involving  $\langle \phi_{cL}|\phi_{vR} \rangle$  and  $\langle \phi_{c'R}|\phi_{vL} \rangle$  (and the corresponding terms with  $\phi_{vL}$ ) dominate. As  $R$  decreases to the size of  $\phi_v$  (i.e., when the charge distribution of the incoming He atom starts penetrating the  $\phi_v$  orbital), the two-center overlap stops increasing so

<sup>†</sup> For two orbitals  $\phi_a$  and  $\phi_b$  located on different centers, the interatomic potential for large  $R$  is dominated by an exchange term  $K_{ab}$  containing both one-electron (kinetic energy and nuclear attraction) and two-electron (electron repulsion) contributions. If  $\phi_a$  and  $\phi_b$  overlap, the one-electron terms usually dominate and the one- and two-electron terms generally lead to opposite signs. In the case that a and b are coupled as in fig. 1a, the one-electron terms are attractive whereas for orbitals in different rows of fig. 1b, c the one-electron terms are repulsive at large  $R$ .

rapidly. For shorter  $R$  the interactions of  $\phi_{cR}$  with  $\phi_{cL}$  and  $\phi_{c'L}$  (and  $\phi_{cL}$  with  $\phi_{cR}$  and  $\phi_{c'R}$ ) start dominating the energy. The energy curve begins to resemble the corresponding curve for He<sub>2</sub><sup>+</sup>, and the total energy may start to decrease. Thus, qualitatively, it is easy to understand how energy humps would be characteristic of the excited states of He<sub>2</sub>. From this argument we would expect the location of the hump to correspond approximately to the sum of the radii of the interacting diffuse and core orbitals. Thus we expect humps at  $\approx 2.2 \text{ Å}^\ddagger$  for  $v = 2s$ . Now, however, we must examine the calculated wavefunctions to see how well such a simple interpretation agrees with the ab initio results.

First, to determine whether self-consistent effects are important in determining the shape of the potential curve, we consider a wavefunction of the GVB form (figs. 1d and 1e) but in which each orbital is forced to retain the shape appropriate to  $R = \infty$ , i.e., each orbital is an atomic orbital. This wavefunction is referred to as the *frozen orbital* (FO) wavefunction. The results are shown by the dotted and dashed lines of fig. 2. We see that at large  $R$  both the A and C curves are repulsive but that the A state leads to a hump near 2.6 Å (4.9  $a_0$ ) and a minimum near  $R = 1.2 \text{ Å}$  (2.3  $a_0$ ). Thus for the A state the frozen orbital wavefunction accounts for the shape of the potential surface<sup>††</sup> and the above discussion (which assumed a frozen orbital wavefunction) constitutes a pertinent rationalization of the state.

In contrast, the frozen orbital wavefunction leads to a purely repulsive potential for the C state [13]. This behavior can be understood by examining the form of the wavefunction in fig. 1d for  $R$  less than the size of  $\phi_v$ , but larger than the size of the core orbitals. In this case  $\phi_{vR} \approx \phi_{vL}$  and the wavefunction can be written as in fig. 1f. Factoring  $\phi_v$  out of the wavefunction leads to a three-electron wavefunction of the form shown in fig. 1g<sup>‡</sup>, which describes the  $2\Sigma_g^+$  state of He<sub>2</sub><sup>+</sup>. On the other hand, the same procedure

<sup>†</sup> The "size" of the orbitals here is defined, somewhat arbitrarily, as  $\langle r^2 \rangle^{1/2}$ .

<sup>††</sup> Buckingham and Dalgarno [13] carried out a calculation comparable to the FO calculation reported here except that each orbital was represented by a single Slater function. They also found a hump for the A state and a repulsive curve for the C state.

<sup>‡</sup> For footnote see next page.

for the A state (fig. 1e) leads to the wavefunction shown in fig. 1h, which describes the  ${}^2\Sigma_u^+$  state of  $\text{He}_2^+$ . These three-electron states (figs. 1g and 1h) are just the anti-resonant and resonant VB states of  $\text{He}_2^+$  and lead to a repulsive curve for  ${}^2\Sigma_g^+$  and bonding for  ${}^2\Sigma_u^+$ . Thus for small  $R$  (so that  $\phi_{vI} \approx \phi_{vR}$ ) the interaction of the core orbitals is attractive for the A state and repulsive for the C state. This then is added to the weakly repulsive interaction due to the interactions of  $\phi_{vR}$  and  $\phi_{vI}$  with the core orbitals on the opposite He to account for the shapes of the frozen curves of fig. 2.

Starting with  $\phi_v = 2p\sigma$ , the same arguments would predict a repulsive interaction at large  $R$  in both the  ${}^1\Sigma_g^+$  and  ${}^1\Sigma_u^+$  states. However, for small  $R$  we obtain  $\phi_{vI} \approx -\phi_{vR}$ , and we can write the wavefunctions as in figs. 1j and 1k. Thus it is the  ${}^1\Sigma_g^+$  state that leads to attractive  $\text{He}_2^+$  interactions and the  ${}^1\Sigma_u^+$  state that leads to repulsive  $\text{He}_2^+$  interactions. Indeed, the frozen orbital energies for these states (see fig. 2, dashed lines) show just this effect<sup>‡</sup>. As a consequence the  ${}^1\Sigma_g^+$  frozen orbital curves arising from the  $\phi_v = 2s$  and  $\phi_v = 2p$  states cross. As shown in fig. 3 the self-consistent calculation leads to orbitals that change continuously between the 2s and 2p limits. Thus the C state is repulsive at large  $R$  due to the  $\phi_{vR}, \phi_{vI} = 2s$  interactions with the core orbitals on the opposite He. It is more repulsive than the A state because of the difference in the nature of the  $\text{He}_2^+$  interactions but finally becomes attractive at small  $R$  because of the crossing with the 2p  ${}^1\Sigma_g^+$  state (i.e., inclusion of favorable  $\text{He}_2^+$  interactions). Thus for the C state the crossing point occurs at smaller  $R$  than the position of the maximum in the A state and in addition the hump is much larger than for the A state.

In the case that  $\phi_v = 2p\pi$  the unfavorable interaction between  $\phi_{vR}$  and  $\phi_{vI}$  orbital vanishes (the unfavorable terms are related to the overlaps which are now zero) and hence the lowest singlet state should be  ${}^1\Pi_g$  (i.e.,  ${}^2\Sigma_u \times {}^2\Pi_u$ ) and should not lead to a hump, while the  ${}^1\Pi_u$  state (i.e.,  ${}^2\Sigma_g \times {}^2\Pi_u$ ) is repulsive since it involves  ${}^2\Sigma_g^+$ -type  $\text{He}_2^+$  interactions (it

eventually crosses the attractive  ${}^1\Pi_u$  curve arising from the 3  ${}^1D$  leading to a shape similar to C  ${}^1\Sigma_g^+$ ). Similar analyses follow for the higher states<sup>†</sup>.

For  ${}^3\Sigma$  states the spin coupling (see fig. 1l) again leads to repulsive interactions at large  $R$ . In addition, for  $R$  small enough that  $\phi_{vR} \approx \phi_{vI}$  these states lead to the same combinations of  ${}^2\Sigma_u^+$  and  ${}^2\Sigma_g^+$  components (of  $\text{He}_2^+$ ) as for the  ${}^1\Sigma$  states. Thus the  ${}^3\Sigma$  states should behave quite similarly to the  ${}^1\Sigma$  states (except that there is no state analogous to X  ${}^1\Sigma_g^+$ ).

## 5. Comparisons with other interpretations

A common explanation of humps in potential curves is in terms of a crossing of two potential curves of the same system. Higher order corrections split the crossing states and lead to a hump in the lower curve. We saw above that this indeed is a viable explanation of the large hump occurring in the C  ${}^1\Sigma_g^+$  state. However, there is no state at all close to the A  ${}^1\Sigma_u^+$  state and indeed the frozen orbital wavefunction also leads to the hump. Hence, curve crossing cannot be an explanation here.

For  $\text{He}_2$  Mulliken [17] suggested that the hump occurs, e.g., in C  ${}^1\Sigma_g^+$ , because the 2s orbital of the separated atoms system correlates with the 3p orbital of the united atom, forcing the valence orbital to be promoted in forming the molecule. However, we found that the repulsive part of the C state curve is well described by the frozen wavefunction which allows for no promotional effect. In addition, we find that the self-consistent GVB orbitals for the C state lead to a continuous change from 2s character at large  $R$  to 2p character near  $R_e$ . Thus the promotional effect does *not* appear to be important in leading to these energy humps.

## 6. Conclusion

The potential curves for the  ${}^1\Sigma$  excited states of  $\text{He}_2$  arising from  $\text{He} + \text{He}^*$  ( $n = 2$ ) are repulsive at large

<sup>‡</sup> The four-electron wavefunction is obtained from the wavefunctions of the form shown in figs. 1g or 1h by multiplying by  $\phi_v$ , including the spin function, and antisymmetrizing.

<sup>†</sup> Note that the frozen  $v = 2p, {}^1\Sigma_u^+$  curve in fig. 2 may provide a route for the dissociative recombination of  $\text{He}_2^+$  with an electron to give  $\text{He}(1s, 2p), {}^1P$ . This is presently being investigated. For experimental results, see ref. [14].

<sup>†</sup> This description is confirmed by extensive CI calculations performed by Gupta and Matsen [15] (for the  ${}^1\Pi_u$  curves arising from  $v = 2p\pi, 3p\pi, 3d\pi$ ) and by Gupta et al. [16] (for the  $v = 2p {}^1\Pi_g$  and  ${}^1\Pi_u$  curve).

$R$  due to the (non-bonding) repulsion of singlet pairs on different centers. Of the two couplings resulting from a specific excited state of He, one leads to attractive  $\text{He}_2^+$ -like core-core interactions and one leads to repulsive core-core interactions. The sign of the resulting interaction depends upon the symmetry of  $\phi_v$ ; e.g.,  $^1\Sigma_u^+$  is favorable for  $v = 2s, 3s, 3d$  and  $^1\Sigma_g^+$  is favorable for  $v = 2p, 3p, 4f$ . As a result, most of the  $\Sigma$  potential energy curves should have at least one hump.

† A more detailed description of the work reported here including calculations on several higher states and an analysis of the repulsions at large  $R$  in terms of exchange effects is presently in preparation.

## References

- [1] R.A. Buckingham, *Trans. Faraday Soc.* 54 (1958) 453.
- [2] W.A. Goddard III et al., *Phys. Rev.* 157 (1967) 81; *J. Am. Chem. Soc.* 93 (1971) 6750.
- [3] S. Huzinaga, *J. Chem. Phys.* 42 (1965) 1293.
- [4] K.M. Sando, *Mol. Phys.* 21 (1971) 439.
- [5] A.L. Smith and K.W. Chow, *J. Chem. Phys.* 52 (1970) 1010.
- [6] A.L. Smith, *J. Chem. Phys.* 49 (1968) 4817.
- [7] F.R. Innes, K. Yoshino and Y. Tanaka, *Sixth International Conference on Electronic and Atomic Collisions* (1969) p. 891.
- [8] K.M. Sando and A. Dalgarno, *Mol. Phys.* 20 (1971) 103.
- [9] M.L. Ginter, *J. Chem. Phys.* 42 (1965) 561.
- [10] D.C. Allison, J.C. Browne and A. Dalgarno, *Proc. Phys. Soc. (London)* 89 (1966) 41.
- [11] D.R. Scott, E.M. Greenawalt, J.C. Browne and F.A. Matsen, *J. Chem. Phys.* 44 (1966) 2981.
- [12] J.C. Browne, *J. Chem. Phys.* 42 (1965) 2826.
- [13] R.A. Buckingham and A. Dalgarno, *Proc. Roy. Soc. A* 213 (1952) 327.
- [14] W.W. Robertson, *J. Chem. Phys.* 42 (1965) 2064.
- [15] B.K. Gupta and F.A. Matsen, *J. Chem. Phys.* 50 (1969) 3797.
- [16] B.K. Gupta et al., *Bull. Am. Phys. Soc.* 12 (1967) 182.
- [17] R.S. Mulliken, *Phys. Rev.* 136 (1964) A962.